Available online at www.sciencedirect.com
SCIENCE DIRECT
Journal of Solid State Chemistry 179 (2006) 1375–1382
JOURNAL OF SOLID STATE CHEMISTRY
www.elsevier.com/locate/jssc

Charge and structural ordering in the brownmillerite phases: $La_{1-x}Sr_xMnO_{2.5}$ ($0.2<x<0.4$)

Peter S. Casey, Daniel Barker, Michael A. Hayward*

Inorganic Chemistry Laboratory, Department of Chemistry, University of Oxford, South Parks Road, Oxford, OX1 3QR, UK

Received 21 November 2005; received in revised form 23 January 2006; accepted 27 January 2006
Available online 28 February 2006

Abstract

The topotactic reduction of $La_{1-x}Sr_xMnO_3$ ($0.2<x<0.4$) perovskite phases to the corresponding $La_{1-x}Sr_xMnO_{2.5}$ brownmillerite phases with NaH is described. Neutron and electron diffraction data show the $x=0.25$ and 0.2 phases adopt structures with an unusual ordered L–R–L–R alternation of twisted chains of Mn(II) tetrahedra within each anion-deficient layer. This is accompanied by Mn(II)/(III) charge ordering within the remaining MnO_6 octahedral layers. In contrast, the $x=0.4$ phase adopts a structure in which the twisted chains of tetrahedra are disordered.

Keywords: Brownmillerite; Topotactic reduction; Manganese

1. Introduction

Complex manganese oxides have received considerable attention due to the observation of large magnetoresistive ratios in these phases [1–3]. Interest has been sustained by the broader observation of strong coupling between spin, charge and lattice degrees of freedom [4,5]. The report of unusually large magnetoresistive effects in the brownmillerite phase $SrCaMnGaO_{5.04}$ [6] has directed interest towards materials of this structural type.

The brownmillerite structure is one of the most common anion-vacancy ordered structures. It can be viewed as an anion-deficient variant of the ABO_3 cubic perovskite structure in which half the anions have been removed from alternate BO_2 layers. This gives the stacking sequence AO–BO_2–AO–BO–AO– with alternating layers of apex-linked BO_6 octahedra and BO_4 tetrahedra as shown in Fig. 1.

The anion vacancies are arranged within the BO layers in an ordered manner to yield chains of vacancies parallel to the [110] direction of the simple cubic perovskite lattice. The resulting layers consist of chains of apex-linked BO_4 units which also run along the [110] direction. The structure is complicated by the possibility that the chains of tetrahedra can undergo a cooperative twist, which can occur in either a clock-wise or anti-clockwise sense, to yield 'left'- or 'right'-handed chains (Fig. 2)—the two being related by symmetry.

The three-dimensional arrangement of the twisted chains of tetrahedra leads to a number of general structural configurations (Fig. 3): the *Ima*2 configuration in which all the chains are twisted in the same direction; the *Pnma* configuration where all the chains within the same layer are twisted in the same direction, but the twist direction is inverted between adjacent layers; disordered configurations in which there is a random arrangement of twisted chains. A fourth arrangement has also been observed in which an alternating arrangement of 'left'- and 'right'-handed chains of tetrahedra exists within the same layer as shown in Fig. 3 ($P2_1/c$ configuration). Significant efforts have been made to characterise the structural configurations adopted by A_2MnBO_{5+x} ($A=$ Ca, Sr; $B=$ Ga, Al) phases and to relating these with the often complex magnetic behaviour of the materials to gain a better understanding of the magnetic exchange interactions present in these phases [7–11].

In recent work, it has been shown that binary metal hydrides can affect the topotactic deintercalation of oxide

*Corresponding author. Fax: +44 1865 272690.
E-mail address: michael.hayward@chem.ox.ac.uk (M.A. Hayward).

0022-4596/$ - see front matter © 2006 Elsevier Inc. All rights reserved.
doi:10.1016/j.jssc.2006.01.049

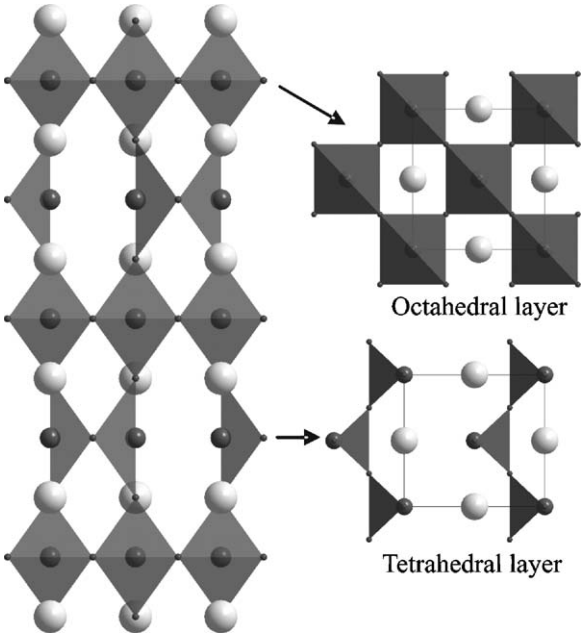

Fig. 1. The brownmillerite structure. Insets show views of the octahedral and tetrahedral layers.

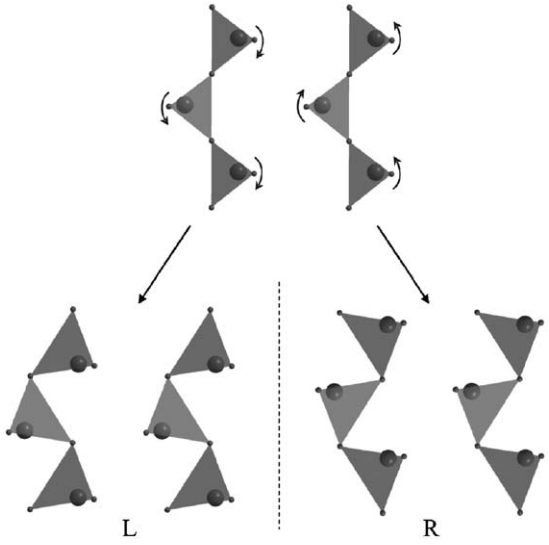

Fig. 2. Cooperative twisting of the chains of tetrahedra leads to two, symmetry-related, distorted chains.

ions from complex manganese oxides to yield phases with mean manganese oxidation states between Mn(II) and Mn(III) [12]. The topotactic reduction of $Ln_{1-x}A_xMnO_3$ (Ln = lanthanide, A = Ca, Sr) perovskites by this method offers a route to prepare the 'all-manganese' brownmillerite phases $Ln_{1-x}A_xMnO_{2.5}$ thus enabling a direct comparison with the A_2MnBO_{5+x} phases.

2. Experimental

Five-gram samples of $La_{1-x}Sr_xMnO_3$ ($x = 0.2$, 0.25, 0.4) were prepared via a citrate gel method. Suitable ratios of

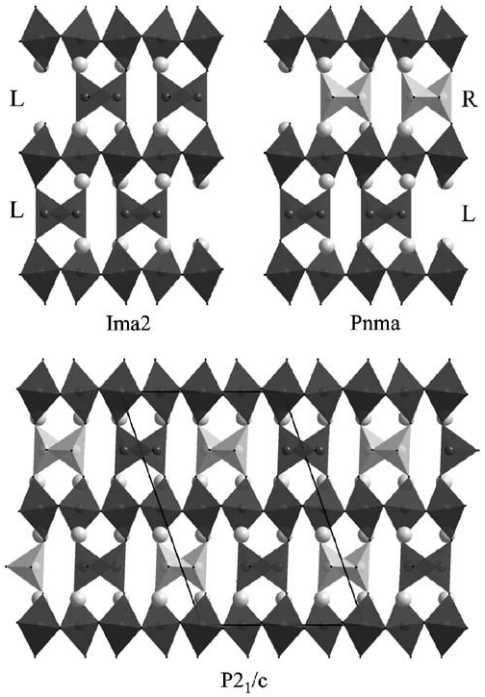

Fig. 3. Ordered arrangements of the two types of twisted chains of tetrahedra.

La_2O_3 (99.999%, dried at 900 °C), $SrCO_3$ (99.994%) and MnO_2 (99.999%) were dissolved in a minimum quantity of a 1:1 mixture of 6 M nitric acid and distilled water. Two mole equivalents of citric acid and 5 ml of analar ethylene glycol were added and the solution heated with constant stirring. The gel thus formed was subsequently ground into a fine powder, placed in an alumina crucible and heated at 1 °C min^{-1} to 1000 °C in air. Samples were then reground and pressed into 13 mm pellets under 5 tonne pressure and heated in air for three periods of 2 days at 1300 °C with regrinding between heating periods. Samples were observed to be phase pure, by laboratory X-ray powder diffraction with lattice parameters in good agreement with published values [13].

The reduction of samples was performed using NaH (Aldrich >95%). $La_{1-x}Sr_xMnO_3$ samples were thoroughly ground in an Argon filled glove box (O_2 and H_2O <1 ppm) with a double stoichiometric quantity of NaH. The resulting mixtures were then sealed in evacuated Pyrex tubes and heated for three periods of 3 days at 210 °C with grinding between heating periods. Samples were then washed with 4 × 100 ml of methanol under nitrogen to remove sodium containing phases (NaOH and NaH) before being dried under vacuum.

Thermogravimetric data were collected from powdered samples heated under flowing oxygen using a Rheometric Scientific STA 1500 thermal analyser. Neutron powder diffraction data were collected from samples contained in vanadium cans sealed with an indium washer under an argon atmosphere. Data were collected at room temperature from the $x = 0.25$ and 0.4 samples using the D2b

Table 1
Refined orthorhombic and monoclinic lattice parameters of $La_{1-x}Sr_xMnO_{2.5}$

Phase	Orthorhombic—*Pnma*			Monoclinic—$P2_1/c$			
	a (Å)	*b* (Å)	*c* (Å)	*a* (Å)	*b* (Å)	*c* (Å)	β (deg)
0.4	5.4198(3)	16.6219(8)	5.5170(3)	11.0345(6)	5.4199(3)	17.517(1)	108.38(1)
0.25	5.4961(1)	16.3353(5)	5.6514(1)	11.3032(3)	5.4959(1)	17.2879(9)	109.109(8)
0.2	5.5162(6)	16.294(1)	5.6665(6)	11.333(1)	5.5165(6)	17.250(2)	109.159(6)

diffractometer ($\lambda = 1.59$ Å) at the ILL, Grenoble and from the $x = 0.2$ sample using POLARIS at the ISIS, UK. Reitveld profile refinement against the diffraction data was performed using the GSAS suite of programs [14]. Electron diffraction patterns were collected from samples supported on lacy carbon grids (deposited from suspension in methanol) using a JEOL 2000FX microscope operating at 200 kV.

3. Results

Thermogravimetric re-oxidation data collected from the reduced samples was consistent with the composition $La_{1-x}Sr_xMnO_{2.50(3)}$ for all three samples. Complete oxidation back to $La_{1-x}Sr_xMnO_{3.00}$ was confirmed by X-ray powder diffraction. Neutron powder diffraction data collected from all three $La_{1-x}Sr_xMnO_{2.5}$ samples could be readily indexed on the basis of orthorhombic unit cells (Table 1) related to a simple cubic perovskite cell, by the expansion $a' \approx \sqrt{2} \times a$, $b' \approx 4 \times b$, $c' \approx \sqrt{2} \times c$, suggesting a brownmillerite-type structure (Fig. 4). The observation of strong (201) reflections in the diffraction data indicated a primitive rather than body-centred space group, therefore models based on ordered *Pnma*-type brownmillerite structures were refined against the neutron diffraction data. The agreement between observed and calculated diffraction patterns from these models were reasonable (Table 2); however, close inspection of the refined models revealed some highly anisotropic displacement parameters, particularly for the 'equatorial' oxide ions in the tetrahedral MnO layers. This suggests that a strict *Pnma*-type ordering of the tetrahedral chain twisting is a poor description of these phases.

In order to unambiguously determine the unit cells and space groups of the $La_{1-x}Sr_xMnO_{2.5}$ phases, selected area electron diffraction data were collected. Figs. 5a and b show electron diffraction patterns collected from $La_{0.6}Sr_{0.4}MnO_{2.5}$, which can be readily indexed as the [010] and [101] zones of the unit cell described in Table 1. Similarly Figs. 5c and e can be readily indexed as the $[1\bar{1}3]$ and $[3\bar{1}3]$ zones of the same orthorhombic cell. Figs. 5d and f show the corresponding zones from the $x = 0.25$ sample which are identical to the $x = 0.4$ data but with an additional set of diffraction reflections which show a doubling along the [031] direction. The smallest unit cell consistent with these additional diffraction reflections is the monoclinic cell described in Table 1 and related to the orthorhombic cell as shown in Fig. 4. Assuming the cell expansion is due to a change in the ordering of the twist directions of the chains of tetrahedra, the monoclinic cell produced, and the compatibility with the $P2_1/c$ space

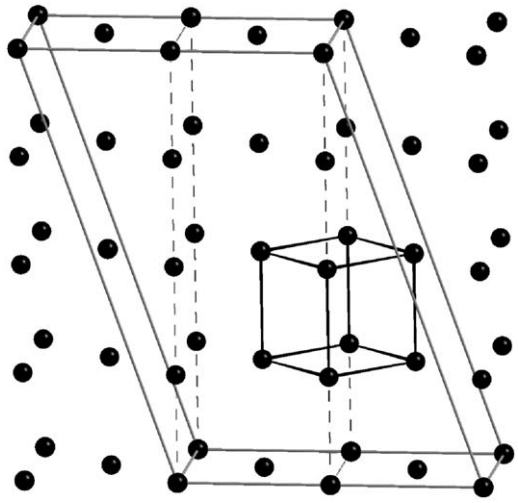

Fig. 4. The geometric relationship between the simple cubic perovskite, orthorhombic brownmillerite (dashed lines) and monoclinic brownmillerite unit cells. Spheres show the positions of the manganese ions.

Table 2
Statistical fitting parameters from structural refinement of different models against neutron powder diffraction data collected for $La_{1-x}Sr_xMnO_{2.5}$ phases

Model	χ^2	wR_p	R_p
$La_{0.6}Sr_{0.4}MnO_{2.5}$			
Ordered *Pnma*	4.681	4.84	3.66
Disordered *Pnma*	**3.695**	**4.24**	**3.21**
$P2_1/c$	4.276	4.64	3.55
$La_{0.75}Sr_{0.25}MnO_{2.5}$			
Ordered *Pnma*	3.642	3.79	2.88
Disordered *Pnma*	3.276	3.61	2.78
P*2₁/*c	**2.851**	**3.37**	**2.64**
$La_{0.8}Sr_{0.2}MnO_{2.5}$			
Ordered *Pnma*	3.418	3.69	4.83
Disordered *Pnma*	2.273	3.01	4.07
P*2₁/*c	**2.163**	**2.93**	**4.00**

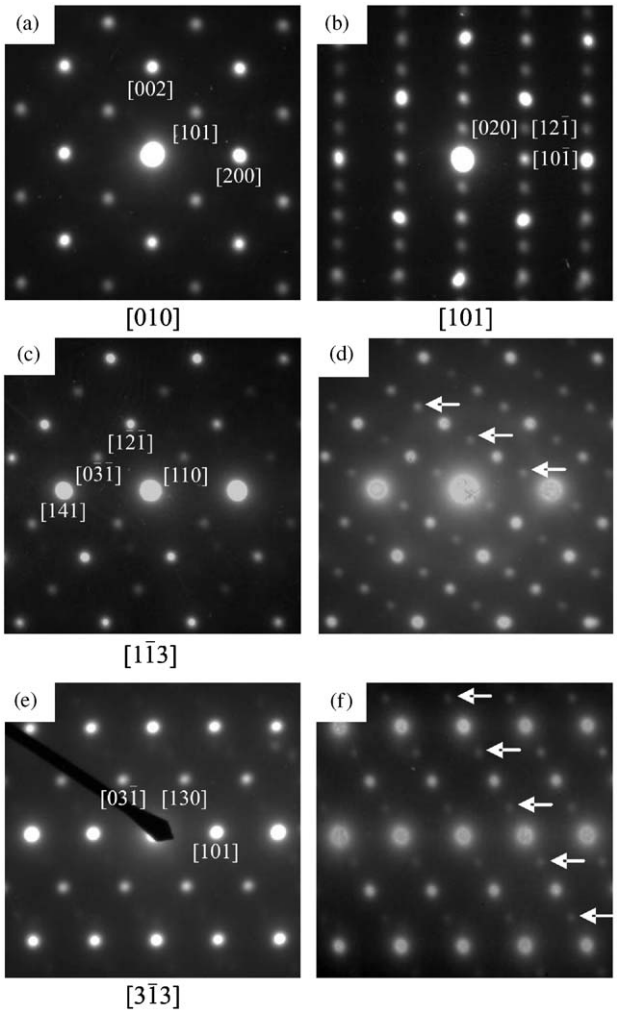

Fig. 5. Electron diffraction data collected from $x = 0.4$ (a, b, c, and e) and $x = 0.25$ (d and f) samples. Additional diffraction features (marked with arrows) present in (d) and (f) compared to (c) and (e) show a doubling of the [031] direction consistent with an expansion to a monoclinic unit cell for the $x = 0.25$ phase.

group, suggests an alternating sequence of left and right twisted chains within layers as well as between layers as suggested for Sr_2MnGaO_5 [11,15] and shown in Fig. 3. Such a model was constructed in the $P2_1/c$ space group and refined against the neutron diffraction data. Atomic constraints were used to impose a strict symmetry relationship between the left and right twisted tetrahedral chains and are detailed in the Supplementary Information. Refinement proceeded smoothly for the data sets collected from all three samples, goodness of fit parameters are detailed in Table 2.

The data in Table 2 show that the statistical fit to the diffraction data using the ordered monoclinic model is better than that for the ordered *Pnma* model for all samples. There is, however, no direct evidence for a cell expansion for the $x = 0.4$ sample from electron diffraction despite an extensive search. These two apparently contradictory observations suggest that the phase is structurally disordered with the monoclinic model being a better

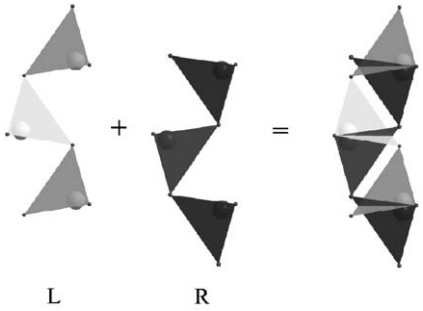

Fig. 6. Disordered superposition of left and right twisted chains of tetrahedra.

approximation to the structure than the ordered *Pnma* model. To test this hypothesis a model was constructed in the *Pnma* space group with a 1:1 superposition of left and right twisted chains of tetrahedra as shown in Fig. 6, and refined against the diffraction data. As noted previously the observation of a strong (201) reflection prevents the use of the standard *Icmm* disordered model.

A comparison of the goodness of fit parameters for all three models (monoclinic, ordered and disordered *Pnma*) given in Table 2, reveals the monoclinic model is preferred for the $x = 0.2$ and 0.25 samples, although in the former case only marginally so, and the disordered *Pnma* model is preferred for the $x = 0.4$ phase.

A final possibility is that multiple ordering regimes exist within the same sample (as observed for $Ca_2MnGaO_{5.04}$ [16]) in response, for example, to slight local variations in La:Sr ratio. In order to investigate this possibility two-phase models, consisting of ordered *Pnma* and *Im2a* structures, were refined against the diffraction data. When allowed to refine freely the phase fraction of the body-centred phase always declined to zero. The same result was also observed when a disordered *Pnma* model was partnered with the body-centred model. Therefore we conclude the $x = 0.4$ phase is best described by a single disordered *Pnma* model.

Statistically the $P2_1/c$ monoclinic structure is clearly preferred over either orthorhombic model for $La_{0.75}Sr_{0.25}MnO_{2.5}$. The case for the $x = 0.2$ phase is less clear as the agreement factors are very similar for the disordered *Pnma* and monoclinic structural descriptions. In order to clarify the situation electron diffraction data collected from the $x = 0.2$ sample were closely examined. Fig. 7 shows one such diffraction pattern which can be readily indexed as the [0$\bar{1}$3] zone axis of an orthorhombic cell. It can be seen that there are a series of additional diffraction features which indicate a doubling of the [031] direction consistent with the described monoclinic expansion. It should be noted, however, that these additional diffraction features are weaker and appear to be extended along the [031] direction. This broadening indicates partial disorder in this phase, and in combination with the similar neutron fitting statistics for the disordered orthorhombic and monoclinic structural models suggests the $x = 0.2$

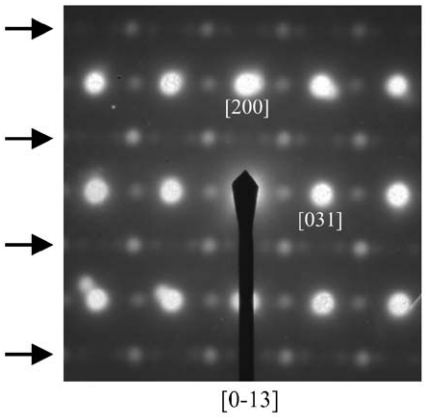

Fig. 7. Electron diffraction data collected from the $x = 0.2$ sample indexed as the [0$\bar{1}$3] zone of a orthorhombic cell. Additional diffraction reflections indicate a doubling of the [031] direction; however, there is also significant disorder in this direction as indicated by arrows.

phase is on the cusp of a change in structure, but on the grounds of the neutron fitting statistics the monoclinic model is preferred. Tables 3–5 detail the final refined models for the three $La_{1-x}Sr_xMnO_{2.5}$ phases with the fits to the data shown in Fig. 8. Metal–oxygen bond lengths are given in Tables 6 and 7.

4. Discussion

Reaction of $La_{1-x}Sr_xMnO_3$ ($0.2 < x < 0.4$) with NaH results in the topotactic deintercalation of oxide ions to form phases of composition $La_{1-x}Sr_xMnO_{2.5}$ which adopt brownmillerite structures. The adoption of a brownmillerite structure for an anion-deficient manganese oxide is a little unexpected. $Ca_2Mn_2O_5$ [17] and $Sr_2Mn_2O_5$ [18] are also prepared by the topotactic reduction of $AMnO_3$ perovskites and adopt structures containing arrays of apex-linked MnO_5 square-based pyramidal units as does the

Table 3
Structural parameters refined from neutron powder diffraction data collected at room temperature from $La_{0.6}Sr_{0.4}MnO_{2.5}$

		x	y	z	Fraction	U_{iso}
La/Sr	8*d*	0.003(2)	0.11244(9)	0.4889(5)	0.6/0.4	0.0121(8)
Mn	4*a*	0	0	0	1	0.013(1)
Mn	4*c*	0.037(2)	0.25	0.944(1)	0.5	0.015(2)
Mn	4*c*	0.966(2)	0.25	0.944(1)	0.5	0.015(2)
O	8*d*	0.994(2)	0.1345(1)	0.0404(6)	1	0.020(1)
O	8*d*	0.252(2)	0.9915(2)	0.236(1)	1	0.016(1)
O	4*c*	0.070(1)	0.25	0.579(1)	0.5	0.028(2)
O	4*c*	0.429(1)	0.25	0.920(1)	0.5	0.028(2)

Space group: *Pnma*. $a = 5.4198(3)$ Å, $b = 16.6219(8)$ Å, $c = 5.5170(3)$ Å, volume $= 497.02(7)$ Å^3, $\chi^2 = 3.695$, w$R_p = 4.24\%$, $R_p = 3.21\%$.

Table 4
Structural parameters refined from neutron powder diffraction data collected at room temperature from $La_{0.75}Sr_{0.25}MnO_{2.5}$

		x	y	z	Fraction	U_{iso}
La/Sr(1)	4*e*	0.0647(6)	0.5006(9)	0.11173(6)	0.75/0.25	0.0099(3)
La/Sr(2)	4*e*	0.2991(6)	0.0006(9)	0.11173(6)	0.75/0.25	0.0099(3)
La/Sr(3)	4*e*	0.5647(6)	0.5006(9)	0.11173(6)	0.75/0.25	0.0099(3)
La/Sr(4)	4*e*	0.7991(6)	0.0006(9)	0.11173(6)	0.75/0.25	0.0099(3)
Mn(1)	2*a*	0	0	0	1	0.0087(7)
Mn(2)	2*b*	0.5	0	0	1	0.0087(7)
Mn(3)	4*e*	0.75	0.5	0	1	0.0087(7)
Mn(4)	4*e*	0.5985(3)	0.0424(9)	0.25	1	0.0087(7)
Mn(5)	4*e*	0.9014(3)	0.4575(9)	0.25	1	0.0087(7)
O(1)	4*e*	0.0759(4)	0.5788(6)	0.2473(7)	1	0.0169(5)
O(2)	4*e*	0.5759(4)	0.4211(6)	0.2473(7)	1	0.0169(5)
O(3)	4*e*	0.8727(5)	0.245(1)	0.0106(1)	1	0.0169(5)
O(4)	4*e*	0.8772(5)	0.745(1)	0.0106(1)	1	0.0169(5)
O(5)	4*e*	0.6227(5)	0.254(1)	0.9893(1)	1	0.0169(5)
O(6)	4*e*	0.6272(5)	0.754(1)	0.9893(1)	1	0.0169(5)
O(7)	4*e*	0.7821(1)	0.5207(7)	0.1371(1)	1	0.0169(5)
O(8)	4*e*	0.5928(1)	0.0207(7)	0.1371(1)	1	0.0169(5)
O(9)	4*e*	0.2821(1)	0.5207(7)	0.1371(1)	1	0.0169(5)
O(10)	4*e*	0.0928(1)	0.0207(7)	0.1371(1)	1	0.0169(5)

Space group: $P2_1/c$. $a = 11.3032(3)$ Å, $b = 5.4959(1)$ Å, $c = 17.2879(9)$ Å, $\beta = 109.109(8)^\circ$, volume $= 1014.77(6)$ Å^3, $\chi^2 = 2.851$, w$R_p = 3.37\%$, $R_p = 2.64\%$.

Table 5
Structural parameters refined from neutron powder diffraction data collected at room temperature from $La_{0.8}Sr_{0.2}MnO_{2.5}$

		x	y	z	Fraction	U_{iso}
La/Sr(1)	4*e*	0.0600(2)	0.5038(3)	0.11213(3)	0.8/0.2	0.0007(2)
La/Sr(2)	4*e*	0.2962(2)	0.0038(3)	0.11213(3)	0.8/0.2	0.0007(2)
La/Sr(3)	4*e*	0.56002(2)	0.5038(3)	0.11213(3)	0.8/0.2	0.0007(2)
La/Sr(4)	4*e*	0.7962(2)	0.0038(3)	0.11213(3)	0.8/0.2	0.0007(2)
Mn(1)	2*a*	0	0	0	1	0.0095(4)
Mn(2)	2*b*	0.5	0	0	1	0.0095(4)
Mn(3)	4*e*	0.75	0.5	0	1	0.0095(4)
Mn(4)	4*e*	0.5997(1)	0.0322(5)	0.25	1	0.0095(4)
Mn(5)	4*e*	0.9002(1)	0.4677(5)	0.25	1	0.0095(4)
O(1)	4*e*	0.0755(2)	0.5802(3)	0.2482(4)	1	0.0150(4)
O(2)	4*e*	0.5755(2)	0.4197(3)	0.2482(4)	1	0.0150(4)
O(3)	4*e*	0.8770(2)	0.2541(4)	0.01216(6)	1	0.0150(4)
O(4)	4*e*	0.8729(2)	0.7541(4)	0.01216(6)	1	0.0150(4)
O(5)	4*e*	0.6270(2)	0.2458(4)	0.98783(6)	1	0.0150(4)
O(6)	4*e*	0.6229(2)	0.7458(4)	0.98783(6)	1	0.0150(4)
O(7)	4*e*	0.78255(8)	0.4746(2)	0.13665(6)	1	0.0150(4)
O(8)	4*e*	0.59244(8)	0.9746(2)	0.13665(6)	1	0.0150(4)
O(9)	4e	0.28255(8)	0.4746(2)	0.13665(6)	1	0.0150(4)
O(10)	4*e*	0.09244(8)	0.9746(2)	0.13665(6)	1	0.0150(4)

Space group: $P2_1/c$. $a = 11.333(1)$ Å, $b = 5.5165(6)$ Å, $c = 17.250(2)$ Å, $\beta = 109.159(6)^\circ$, volume $= 1018.8\ (3)$ Å^3, $\chi^2 = 2.163$, w$R_p = 2.93\%$, $R_p = 4.00\%$.

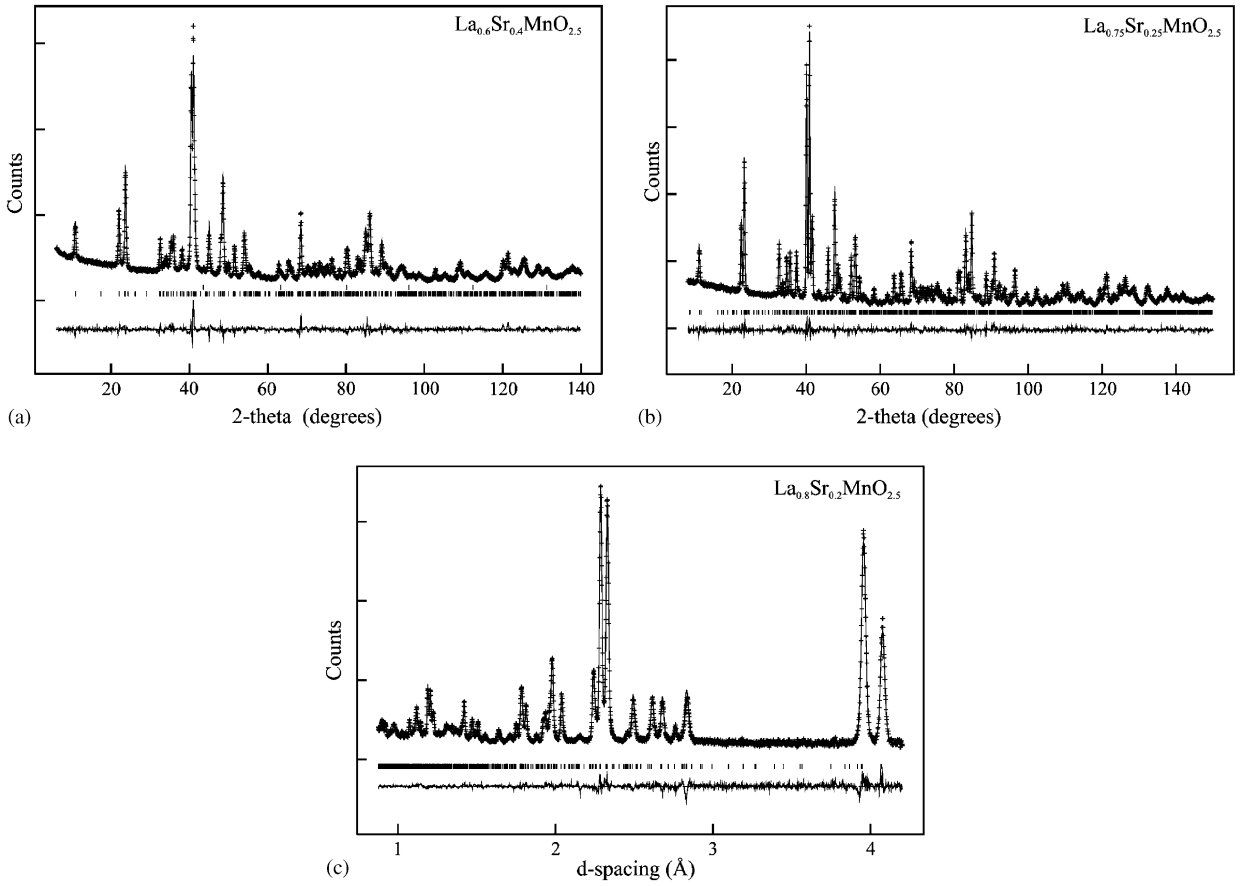

Fig. 8. Observed, calculated and difference plots from the structural refinement of $La_{1-x}Sr_xMnO_{2.5}$ ($x = 0.2$, 0.25, 0.4). The second set of reflection markers in the $x = 0.4$ data correspond to vanadium from the sample container.

analogous Ruddlesden–Popper phase $Sr_3Mn_2O_6$ [19]. The change to the 1:1 mixture of 4-fold and 6-fold coordinations present in the brownmillerite structure is presumably driven by the presence on Mn(II) centres in the $La_{1-x}Sr_xMnO_{2.5}$ phases as has also be observed for $La_{0.5}Ca_{0.5}MnO_{2.5}$ [20]. The unit cell volumes of all phases

Table 6
Metal–oxygen bond lengths obtained from the structural refinement of $La_{0.6}Sr_{0.4}MnO_{2.5}$ (Å)

Mn(1)	O(1) × 2	2.247(2)
	O(2) × 2	1.987(8)
	O(2) × 2	1.892(9)
Mn(2)	O(1) × 2	2.006(3)
	O(4)	2.092(8)
	O(4)	2.12(1)
Mn(3)	O(1) × 2	1.998(3)
	O(3)	2.091(8)
	O(3)	2.15(1)
La/Sr	O(2)	2.570(9)
	O(2)	2.683(9)
	O(2)	2.726(9)
	O(2)	2.794(8)
	O(1)	2.69(1)
	O(1)	2.78(1)
	O(1)	3.066(4)
	O(1)	2.501(4)
	O(3) × 1/2	2.375(3)
	O(4) × 1/2	2.368(3)

Table 7
Metal–oxygen bond lengths obtained from the structural refinement of $La_{0.75}Sr_{0.25}MnO_{2.5}$ and $La_{0.8}Sr_{0.2}MnO_{2.5}$ (Å)

		$x = 0.25$	$x = 0.2$
Mn(1)	O(10)	2.259(8)	2.248(6)
	O(4)	2.023(6)	2.039(2)
	O(3)	2.022(6)	2.036(2)
Mn(2)	O(8)	2.259(8)	2.248(6)
	O(6)	2.026(6)	2.035(2)
	O(5)	2.019(6)	2.038(2)
Mn(3)	O(9)	2.280(3)	2.267(2)
	O(7)	2.280(3)	2.267(2)
	O(4)	1.934(6)	1.938(2)
	O(3)	1.938(6)	1.938(2)
	O(5)	1.939(6)	1.939(2)
	O(6)	1.934(6)	1.939(2)
Mn(4)	O(2)	2.096(7)	2.154(3)
	O(2)	2.096(6)	2.090(3)
	O(9)	1.98(1)	1.998(7)
	O(9)	1.935(2)	1.956(1)
Mn(5)	O(1)	2.096(6)	2.154(3)
	O(1)	2.097(7)	2.091(3)
	O(7)	2.00(1)	1.973(8)
	O(10)	1.962(2)	1.930(1)
La(1)	O(1)	2.34(1)	2.334(7)
	O(10)	2.894(6)	2.638(2)
	O(9)	2.353(8)	2.422(3)
	O(10)	2.676(6)	2.955(2)
	O(3)	2.812(7)	2.810(4)
	O(4)	2.763(7)	2.876(4)
	O(3)	2.69(1)	2.612(8)
	O(4)	2.63(1)	2.641(8)
La(2)	O(2)	2.42(1)	2.41(1)
	O(9)	2.908(6)	2.961(2)
	O(10)	2.512(8)	2.486(3)
	O(9)	2.691(6)	2.644(2)
	O(5)	2.608(8)	2.571(4)
	O(6)	2.553(8)	2.600(4)
	O(4)	2.76(1)	2.712(9)
	O(3)	2.71(1)	2.777(9)
La(3)	O(2)	2.34(1)	2.342(7)
	O(8)	2.894(6)	2.955(2)
	O(7)	2.353(8)	2.422(3)
	O(8)	2.676(6)	2.638(2)
	O(6)	2.810(7)	2.809(4)
	O(5)	2.737(7)	2.875(4)
	O(6)	2.68(1)	2.611(8)
	O(5)	2.63(1)	2.741(8)
La(4)	O(1)	2.42(1)	2.40(1)
	O(7)	2.908(6)	2.961(2)
	O(8)	2.512(8)	2.486(3)
	O(7)	2.691(6)	2.644(2)
	O(4)	2.611(8)	2.571(4)
	O(3)	2.551(8)	2.599(4)
	O(5)	2.76(1)	2.713(9)
	O(6)	2.72(1)	2.778(9)

on reduction increase by around 8% per manganese ion, consistent with the reduction in the mean manganese oxidation state from $Mn(3+x)$ to $Mn(2+x)$.

Calculation of bond valence sums [21,22] around the manganese centres of the reduced phases (Table 8) are consistent with charge ordering between the octahedral and tetrahedral sites—with Mn(II) occupying the tetrahedral sites in all three phases. Bond valence sums around the octahedral site of the $x = 0.4$ phase are consistent with the value of $Mn + 2.8$ predicted by the sample stoichiometry. The situation within the octahedral layers of the $x = 0.25$ and 0.2 samples is more complex. Two of the three octahedral sites in these phases (Mn(1) and Mn(2)) exhibit significantly lower bond valence sums than the remaining Mn(3) site. Additionally, the Mn(3) site is significantly more distorted than either Mn(1) or Mn(2) (axial/equatorial bond length ratios Mn(1), $Mn(2) = 1.11$, $Mn(3) = 1.17$). This suggests a further charge ordering within the octahedral layers in which Mn(II) centres are located at Mn(1) and Mn(2) with a Jahn-Teller distorted Mn(III) centre located on Mn(3). The structural distinction between the Mn(1) and Mn(2) sites and Mn(3) comes from the identity of the chains of tetrahedra to which they are connected. The Mn(1) and Mn(2) sites are connected to like tetrahedral chains—i.e. two 'left'- or two 'right'-handed chains (Fig. 9). This is the situation for all the octahedral sites in *Ima*2 ordered structures (Fig. 3). The Mn(3) site, however, is attached to unlike chains of tetrahedra (one 'left' and one 'right') which is the situation for all the octahedral sites in ordered *Pnma*-type structures. Thus the alternation of 'left'- and 'right'-handed chains within the same tetrahedral layer leads to a rock salt-type charge ordering within the octahedral layers. In the case of $La_{0.75}Sr_{0.25}MnO_{2.5}$ this charge ordering scheme fits the stoichiometry exactly, suggesting that the charge ordering and the need to structurally accommodate the distorted d^4

Table 8
Bond valence sums calculated for manganese centres in $La_{1-x}Sr_xMnO_{2.5}$

Site geometry		$x = 0.4$		$x = 0.25$	$x = 0.2$
Octahedral	Mn(1)	3.02	Mn(1)	2.48	2.42
			Mn(2)	2.48	2.42
			Mn(3)	2.97	2.97
Tetrahedral	Mn(2)	1.96	Mn(4)	2.14	2.11
	Mn(3)	1.96	Mn(5)	2.07	2.02

The sums around octahedral and tetrahedral sites were calculated using the Mn(III) and Mn(II) coefficients, respectively [18].

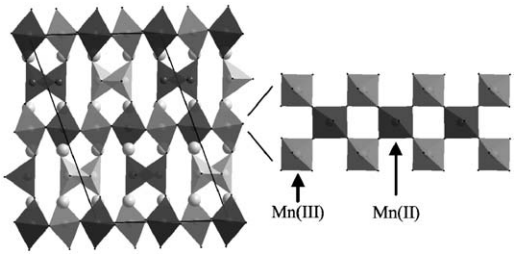

Fig. 9. Charge ordering within the octahedral layers of $La_{0.75}Sr_{0.25}MnO_{2.5}$. Mn(II) sites (dark octahedra) are connected to two tetrahedral chains with the opposing twist directions, Mn(III) sites (light octahedra) are connected to two tetrahedral chains with the same twist direction.

Mn(III) centres is the driving force for the unusual ordering of the twisted chains of tetrahedra. This model also provides an explanation for the proximity of the $x = 0.2$ phase to a structural order/disorder transition—the lowering of the mean manganese oxidation state from Mn + 2.25 to Mn + 2.2 on going from the $x = 0.25$ phase to the $x = 0.2$ phase is sufficient to perturb the rigorous charge ordering within the octahedral layers and thus the ordering of the twist direction of the tetrahedral chains.

5. Conclusion

The topotactic reduction of $La_{1-x}Sr_xMnO_3$ ($0.2 < x < 0.4$) phases at low temperature with NaH yields the corresponding $La_{1-x}Sr_xMnO_{2.5}$ brownmillerite phases. Mn(II)/(III) charge ordering within the octahedral layers of the $x = 0.25$ and 0.2 phases is accompanied by an unusual alternation of the twist direction of the chains of MnO_4 tetrahedra in the anion-deficient layers. Phases which have La:Sr ratios which differ significantly from 3:1 show increasing levels of structural disorder as the rigorous charge ordering is disrupted. The structural relationship between the ordered twisting within the tetrahedral layers and the charge ordering within the octahedral layers suggests this inter-layer interaction could be utilized to order two different *B*-cations within the octahedral layers of brownmillerite oxides. Low-temperature neutron diffraction studies are currently underway to investigate the magnetic behaviour of these new 'all-manganese' brownmillerite phases.

Acknowledgments

We thank R. Smith and E. Suard for assistance collecting neutron powder diffraction data and the Royal Society and the EPSRC for funding this work.

Appendix A. Supplementary Materials

Supplementary data associated with this article can be found in the online version at doi:10.1016/j.jssc.2006.01.049.

References

[1] K. Chahara, T. Ohno, M. Kasao, Y. Kozono, Appl. Phys. Lett. 63 (1993) 1990.
[2] P. Schiffer, A.P. Ramirez, W. Bao, S.-W. Cheong, Phys. Rev. Lett. 75 (1995) 3336.
[3] R. von Helmolt, J. Wecker, B. Holzapfel, L. Schultz, K. Sanwer, Phys. Rev. Lett. 71 (1993) 2331.
[4] M.R. Ibarra, P.A. Algarabel, J. Biasco, J. Garcia, Phys. Rev. Lett. 75 (1995) 3541.
[5] P.G. Radaelli, M. Marezio, H.Y. Hwang, S.-W. Cheong, B. Batlogg, Phys. Rev. B 54 (1996) 8992.
[6] P.D. Battle, A.M.T. Bell, S.J. Blundell, A.I. Coldea, D.J. Gallon, F.L. Pratt, M.J. Rosseinsky, C.A. Steer, J. Solid State Chem. 167 (2002) 188.
[7] A.J. Wright, H.M. Palmer, P.A. Anderson, C. Greaves, J. Mater. Chem. 12 (2002) 978.
[8] A.M. Abakumov, A.S. Kalyuzhnaya, M.G. Rozova, E.V. Antipov, J. Hadermann, G. Van Tendeloo, Solid State Sci. 7 (2005) 801.
[9] V. Pomjakushin, D. Sheptyakov, P. Fischer, A. Balagurov, A. Abakumov, M. Alekseeva, M. Rozova, E. Antipov, D. Khomskii, V. Yushankhai, J. Magn. Magn. Mater 272–276 (2004) 820.
[10] V.Y. Pomjakushin, A.M. Balagurov, T.V. Elzhov, D.V. Sheptyakov, P. Fischer, D.I. Khomskii, V.Y. Yushankhai, A.M. Abakumov, M.G. Rozova, E.V. Antipov, M.V. Lobanov, S.J.L. Billinge, Phys. Rev. B 66 (2002) 184412.
[11] A.M. Abakumov, A.M. Alekseeva, M.G. Rozova, E.V. Antipov, O.I. Lebedev, G. Van Tendeloo, J. Solid State Chem. 174 (2003) 319.
[12] M.A. Hayward, Chem. Commun. (2004) 170.
[13] I.G. Krogh Andersen, E. Krogh Andersen, P. Norby, E. Skou, J. Solid State Chem. 113 (1994) 320.
[14] A.C. Larson, R.B. Von Dreele, General Structural Analysis System, Los Alamos National Laboratory, Los Alamos, 1994.
[15] A.M. Abakumov, M.G. Rozova, B.P. Pavlyuk, M.V. Lobanov, E.V. Antipov, O.I. Lebedev, G. Van Tendeloo, O.L. Ignatchik, E.A. Ovtchenkov, Y.A. Koksharov, A.N. Vasil'ev, J. Solid State Chem. 160 (2001) 353.
[16] A.M. Abakumov, M.G. Rozova, B.P. Pavlyuk, M.V. Lobanov, E.V. Antipov, O.I. Lebedev, G. Van Tendeloo, D.V. Sheptyakov, A.M. Balagurov, F. Bouree, J. Solid State Chem. 158 (2001) 2001.
[17] K.R. Poeppelmeier, M.E. Leonowicz, J.C. Scanlon, J.M. Longo, W.B. Yelon, J. Solid State Chem. 45 (1982) 71.
[18] T. Mori, K. Inoue, N. Kamegashira, Y. Yamaguchi, K. Ohoyama, J. Alloy Compd. 296 (2000) 92.
[19] L.J. Gillie, A.J. Wright, J. Hadermann, G. Van Tendeloo, C. Greaves, J. Solid State Chem. 175 (2003) 188.
[20] J.M. Gonzalez-Calbet, E. Herrero, N. Rangavittal, J.M. Alonso, J.L. Martinez, M. Vallet-Regi, J. Solid State Chem. 148 (1999) 158.
[21] I.D. Brown, D. Altermatt, Acta Crystallogr. Sect. B: Struct. Sci. 41 (1985) 244–247.
[22] N.E. Brese, M. O'Keefe, Acta Crystallogr. Sect. B: Strucut. Sci. 47 (1991) 192–197.